

Chapter 2

Poincaré Recurrences in Ergodic Systems Without Mixing

Vadim Anishchenko, Nadezhda Semenova, Elena Rybalova
and Galina Strelkova

2.1 Introduction

The Poincaré recurrence is one of the fundamental features pertaining to the time evolution of dynamical systems. Recurrence, according to Poincaré, implies that practically any phase trajectory of a set with given probability measure, which leaves a point x_0 of the phase space, will pass infinitely many times arbitrarily close to its initial state as it evolves in time. Poincaré termed this type of motion in dynamical systems as Poisson stable [1].

The statistics of Poincaré recurrences in the global approach has been a topic of research in recent years [2–4]. The local approach idea of the Poincaré recurrence theory consists in calculating Poincaré recurrences in a certain ε -vicinity of a given initial state [5, 6]. In the framework of the global approach, recurrence times are considered in all covering elements of the whole set and their statistics is then analyzed. The main characteristic of the Poincaré recurrence statistics in the global approach is the dimension of return times, which has been introduced in [4] and called as the Afraimovich–Pesin dimension (AP dimension).

V. Anishchenko (✉) · N. Semenova · E. Rybalova · G. Strelkova
Saratov State University, 83, Astrakhanskaya street, Saratov, Russia
e-mail: wadim@info.sgu.ru

N. Semenova
e-mail: semenovani@info.sgu.ru

E. Rybalova
e-mail: eska1706@gmail.com

G. Strelkova
e-mail: strelkovagi@info.sgu.ru

It has been established that the statistics of recurrences in the global approach depends on the topological entropy h_T . Poincaré recurrences have been studied theoretically for mixing sets with $h_T > 0$ [2–4] and the theoretical results have been confirmed by numerical simulation [7–9]. The situation is different in the case of ergodic sets without mixing, i.e., when $h_T = 0$. There are practically no works devoted to studies of the properties of Poincaré recurrences for this case. Some important theoretical results have been obtained in [2–4] for the shift circle (the linear circle map) with an irrational rotation number. In our present work, we aim to study numerically the Poincaré recurrence statistics in the linear and nonlinear circle map with different irrational rotation numbers and to reveal new peculiarities of Poincaré recurrences. The circle map is widely used in nonlinear dynamics to study quasiperiodic oscillations with two independent frequencies.

In the global approach, the whole set of phase trajectories of a dynamical system is covered with cubes (or balls) of size $\varepsilon \ll 1$. A minimal time of the first recurrence of a phase trajectory in the u_i -vicinity $\tau_{\text{inf}}(u_i)$ is calculated for each covering element u_i ($i = 1, 2, \dots, N$). Then, the mean minimal return time is defined over the whole set of covering elements u_i [9–11] as follows:

$$\langle \tau_{\text{inf}}(\varepsilon) \rangle = \frac{1}{N} \sum_{i=1}^m \tau_{\text{inf}}(u_i). \quad (2.1)$$

It has been shown in [2] that in the general case

$$\langle \tau_{\text{inf}}(\varepsilon) \rangle \sim \phi^{-1}(\varepsilon^{\frac{d}{\alpha_c}}) \quad (2.2)$$

where d is the fractal dimension of the considered set, and α_c is the AP dimension of a return time sequence. The gauge function $\phi(t)$ in (2.2) can be given by one of the following forms:

$$\phi(t) \sim \frac{1}{t}, \quad \phi(t) \sim \exp(-t), \quad \phi(t) \sim \exp(-t^2), \dots, \phi(t) \sim \exp(-t^n). \quad (2.3)$$

The appropriate choice of $\phi(t)$ depends on the topological entropy h_T as well as on the multifractality of the considered set if such a property exists. It has been shown in [2, 4] that for $h_T = 0$, the gauge function has an asymptotic form $\phi(t) \sim 1/t$ and the following expression holds

$$\langle \tau_{\text{inf}}(\varepsilon) \rangle \sim \varepsilon^{-\frac{d}{\alpha_c}}, \quad \varepsilon \ll 1. \quad (2.4)$$

For chaotic systems, we have $h_T > 0$ and $\phi(t) \sim \exp(-t)$, and thus, the following law is valid [10]:

$$\langle \tau_{\text{inf}}(\varepsilon) \rangle \sim -\frac{d}{\alpha_c} \ln \varepsilon, \quad \varepsilon \ll 1. \quad (2.5)$$

2.2 Model Under Study

We consider a particular example of a minimal set that is produced by the circle map:

$$\theta_{n+1} = \theta_n + \Delta + K \sin \theta_n, \quad \text{mod } 2\pi \quad (2.6)$$

where Δ and K are the parameters of the map. The circle map of type (2.6) is a reference model of a wide class of dynamical systems with quasiperiodic behavior.

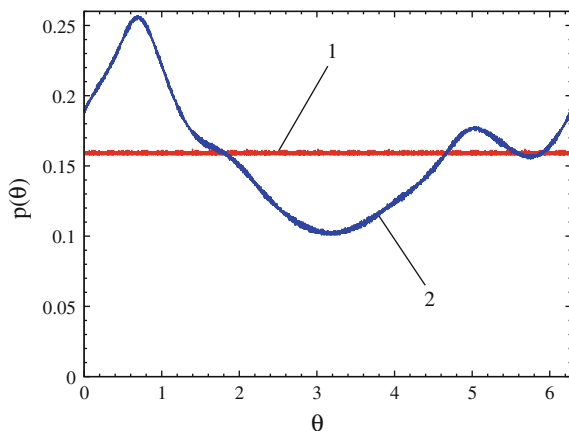
The trajectories of (2.6) are characterized by the rotation number which is defined as the mean increment of angle θ over one iteration of the map with respect to the total angle:

$$\rho = \lim_{n \rightarrow \infty} (\theta_n - \theta_0) / 2\pi n. \quad (2.7)$$

We start by studying the map (2.6) with $K = 0$. In this case, the trajectory rotates by a constant angle Δ per iteration and thus the rotation number can be defined as $\rho = \Delta / 2\pi$. An irrational value of ρ is associated with quasiperiodic trajectories which are everywhere dense on a circle, and the distribution $p(\theta)$ is uniform on the interval $0 \leq \theta_n \leq 2\pi$ (Fig. 2.1). If ρ takes a rational value, i.e., $\rho = k/m$, the trajectory makes k rotations around the circle over m iterations, being a periodic one. In the nonlinear case when $K > 0$, the map cannot already be reduced to rigid rotations of the point on the circle and $p(\theta)$ is no longer uniform (Fig. 2.1).

It has been shown in [2, 4] that the AP dimension of the set $\{\theta_n\}$ which is generated by (2.6) essentially depends on ρ and the methods of its definition.

Fig. 2.1 Distribution density $p(\theta)$ on the circle (2.6) for the golden ratio and with $K = 0.0$ (curve 1) and $K = 0.6$ (curve 2)



All irrational numbers can be divided into transcendental and algebraic numbers. The latter are the numbers that are roots of the equation:

$$C_N \rho^N + \dots + C_1 \rho + C_0 = 0. \quad (2.8)$$

They can be exemplified by $\sqrt[3]{2}$, $\sqrt[3]{3}$, and others where i are natural numbers. The numbers that are not algebraic are said to be transcendental. They include π , e , and $\ln 2$.

Any number can be represented as a continued fraction. In the case of an irrational number, this fraction is infinite and can be written in the form [12]:

$$\rho = a_0 + \frac{1}{a_1 + \frac{1}{a_2 + \frac{1}{\dots}}} \quad (2.9)$$

The sequence of coefficients $\{a_i\}$, $i > 0$, which is written as $[a_0; a_1, a_2, a_3, \dots]$, is called a continued fraction. Irrational values of ρ can be approximated by the ratio of two integers k_i/m_i . That method is said to be the method of rational approximations and the ratio itself is called the i th convergent of a continued fraction. Sequences $\{k_i\}$ and $\{m_i\}$ are increasing, the numerators and denominators are defined using the recursive relations and the coefficients of the continued fraction:

$$\begin{aligned} k_{-1} &= 1, \quad k_0 = a_0, \quad k_i = a_i k_{i-1} + k_{i-2}, \\ m_{-1} &= 0, \quad m_0 = 1, \quad m_i = a_i m_{i-1} + m_{i-2} \end{aligned} \quad (2.10)$$

where $\{a_i\}$ is a sequence of natural coefficients of the continued fraction, k_i and m_i are numerators and denominators of the convergent.

In terms of the convergence rate of rational approximations, irrational numbers can be divided into Diophantine and Liouvillian numbers. The approximation error obeys the inequality:

$$\left| \rho - \frac{k}{m} \right| < \frac{C}{m^\mu} \quad (2.11)$$

where k/m is a convergent from a set of pairs of integers k_i and m_i , $2 \leq \mu < \infty$ is the measure of irrationality, and C is a constant. An irrational rotation number ρ is said to be Diophantine if the upper bound of values of μ for each of which the inequality (2.11) has infinitely many solutions is finite. Otherwise, ρ is a Liouvillian number.

We consider the case of Diophantine approximations of ρ . Following [2, 4], we obtain

$$\left| \rho - \frac{k}{m} \right| \geq \frac{1}{n^{[\nu(\rho)+1+\xi]}} \quad (2.12)$$

where $\nu(\rho) = \sup\{\nu(\rho)\}$ is the maximal rate of Diophantine approximations of an irrational number over all possible pairs of k and m , and $\xi > 0$. It has been proven analytically for (2.12) [2, 4] that

$$\langle \tau_{\inf}(\varepsilon) \rangle \sim \varepsilon^{-\frac{1}{\nu(\rho)}}, \quad \ln \langle \tau_{\inf}(\varepsilon) \rangle \sim -\frac{1}{\nu(\rho)} \ln \varepsilon. \quad (2.13)$$

Here, the fractal dimension of the set $\{\theta_n\}$, which is generated by (2.6), is $d = 1$. Comparing (2.5) and (2.13), we can obtain that $\nu(\rho) = \alpha_c$ in the considered case. This implies that the AP dimension coincides with the approximation rate of the irrational rotation number ρ . Furthermore, the gauge function is $\phi(t) \sim 1/t$. In the following section, we introduce several features of the dependence $\ln \langle \tau_{\inf}(\varepsilon) \rangle$, which are obtained by numerical simulation.

2.3 Main Properties of Return Time Dependence for the Linear Circle Map

We calculate the dependence $\langle \tau_{\inf}(\varepsilon) \rangle$ on the set $\{\theta_n\}$ of the map (2.6) for $K = 0$ and ρ which is equal to the golden ratio:

$$\rho = \frac{1}{2}(\sqrt{5} - 1) \approx 0.618 \dots, \quad \Delta = 2\pi\rho = \pi(\sqrt{5} - 1). \quad (2.14)$$

Since a point rotates uniformly on the circle when $K = 0$, for any interval of ε , there is a single value $\tau_{\inf}(\varepsilon)$ which is independent of the initial point $\theta = \theta_0$. Therefore, we do not need to calculate the mean value (2.1). Numerical results for $\tau_{\inf}(\varepsilon)$ are shown in Fig. 2.2. As shown in the figure, this dependence looks like a step function, which can be referred to as the “Fibonacci stairs.” We have established that it has several features which are as follows.

1. When $\ln \varepsilon$ decreases, the sequence of $\tau_{\inf}(\varepsilon)$ values grows and strictly corresponds to the basic Fibonacci series ($\dots, 8, 13, 21, 34, 55, 89, 144, \dots$): Each subsequent number is the sum of the previous two. The values of τ_{\inf} which relate to the steps of the Fibonacci stairs are indicated in Fig. 2.2.
2. When ε changes within any step of the Fibonacci stairs, three return times $\tau_1 < \tau_2 < \tau_3$ can be distinguished. This property follows from Slater’s theorem [13]. These three return times correspond to the basic Fibonacci series.
3. It has been shown numerically and proven theoretically that lengths and heights of the steps (Fig. 2.2) of the Fibonacci stairs possess a universal property for the golden and silver ratios. The length of the i th step can be defined as follows:

$$D_i = \ln \varepsilon_i - \ln \varepsilon_{i+1} = \text{const} = |\ln \rho|, \quad i \gg 1 \quad (2.15)$$

where ε_i and ε_{i+1} are values of ε at the boundaries of the relevant step. From (2.15), it follows that $\varepsilon_{i+1} = \varepsilon_i \cdot \rho$.

Similarly, for the height of the i th step, we have

$$\ln \tau_{\inf}(\varepsilon_{i+1}) - \ln \tau_{\inf}(\varepsilon_i) = |\ln \rho|, \quad i \gg 1. \quad (2.16)$$

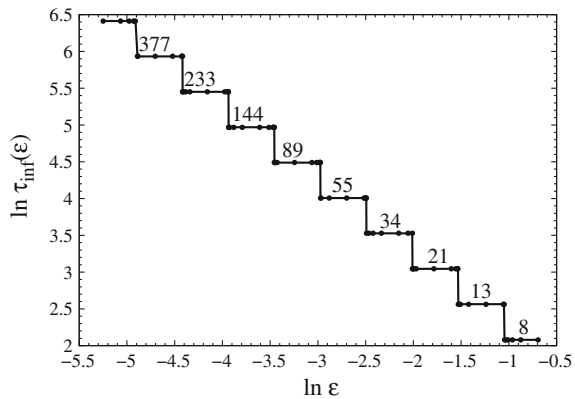
The index i in (2.15) and (2.16) increases as ε decreases (Fig. 2.2). The lengths and the heights of the steps are universal and equal to $|\ln \rho|$ where ρ is the rotation number.

As follows from property 2, when ε changes “within a step,” three return times $\tau_1 < \tau_2 < \tau_3$ can be registered. Its sequence corresponds to the sequence of denominators of convergents, i.e., $\tau_1 = m_i$, $\tau_2 = m_{i+1}$, and $\tau_3 = m_{i+2}$. This implies the appearance of the Fibonacci number sequence in return times. Calculations of probability distributions of return times in different regions of an arbitrary step in the Fibonacci stairs show three different situations. These results are illustrated in Fig. 2.3. We first have $P(\tau_3) < P(\tau_2) < P(\tau_1)$ for the return vicinity which is chosen in the right side of the step (Fig. 2.3a). The change between the three distributions occurs in the middle of the step, i.e., $P(\tau_1) = P(\tau_3) < P(\tau_2)$ (Fig. 2.3b). Finally, $P(\tau_1) < P(\tau_3) < P(\tau_2)$ is observed when the return vicinity is taken in the left half of the step (Fig. 2.3c). At the end of the step the probability $P(\tau_1) \rightarrow 0$ (Fig. 2.3d), a new return time $\tau_4 = m_{i+3}$ is appeared, and the transition to the next step takes place. The distribution in this case is $P(\tau_3) < P(\tau_2) < P(\tau_1)$ (Fig. 2.3e). The minimal return time is already $\tau_{\inf} = \tau_2$ within the next step, and so on.

Now, we try to prove the third property of the Fibonacci stairs which is expressed by the relations (2.15) and (2.16). The validity of (2.15) and (2.16) can be proven by several methods [14–16]. We give one of them.

The structure of Fibonacci stairs is closely related to the theory of convergents and continued fractions. An irrational number is a real number which cannot be written as a fraction k/m where k and m are natural numbers, $1, 2, \dots$

Fig. 2.2 Dependence of the minimal return time $\tau_{\inf}(\varepsilon)$ for the map (2.6) with the golden ratio and for $K = 0$ and $\Delta = 2\pi\rho$



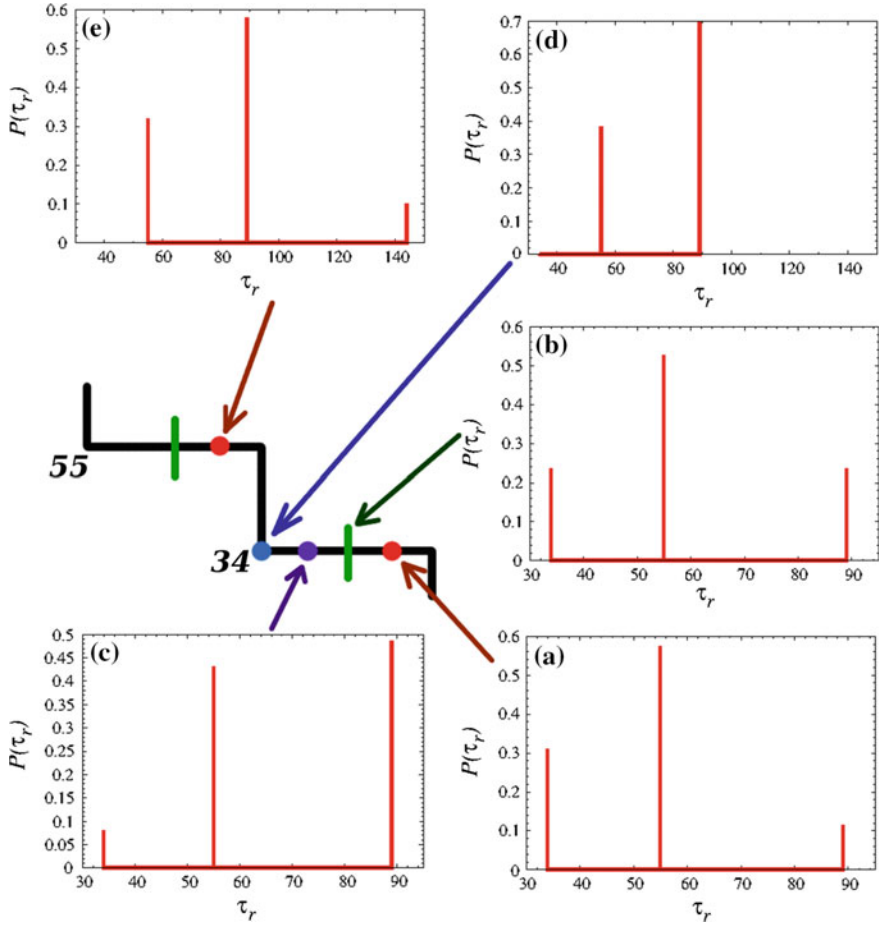


Fig. 2.3 Distributions of return times in the ε -vicinity chosen in different regions of a step of the Fibonacci stairs: **a** at the *right* side, **b** in the *middle*, **c** at the *left* side, **d** at the *left* boundary, and **e** transition to the next step

In the general case, an irrational rotation number can be presented in the form of a continued fraction (2.9). This produces a sequence of approximation coefficients $\{a_i\}$, $i \geq 0$. The notation $[a_0; a_1, a_2, a_3, \dots]$ is an infinite continued fraction representation of the irrational number.

As mentioned in the previous section, the irrational rotation number ρ can be approximated by the fraction of two integers k_i/m_i . This is the method of rational approximations. The i th convergent of the continued fraction $\rho = [a_0; a_1, a_2, a_3, \dots]$ is a finite continued fraction $[a_0; a_1, a_2, \dots, a_i]$, which value is equal to the rational number k_i/m_i . The increasing sequences of numerators $\{k_i\}$ and denominators $\{m_i\}$ are called *continuants* of the i th convergent (2.9) and can be found using fundamental recurrence formulas (2.11).

It has been found [15, 17] that for any rotation number, the dependence $\tau_{\text{inf}}(\varepsilon)$ is a step function and each value $\tau_{\text{inf}i}$, which corresponds to the i th step, is equal to the denominators of the i th convergent k_i/m_i of the rotation number ρ . Using the equality $\tau_{\text{inf}i}(\varepsilon) = m_i$, we obtain the minimal vicinity size which corresponds to this return time $\tau_{\text{inf}i}$. As noted in Introduction, after one iteration of the linear circle map (2.6), the position of the point on the circle changes by $2\pi\rho$. The expression $\tau_{\text{inf}}(\varepsilon) = m_i$ means that the point returns in the neighborhood of its initial state after m_i iterations, shifting by $2\pi\rho m_i$. During these iterations, the point can make several complete circles and appear to the left or right of the initial state. To take this fact into account, we introduce the modulus and subtract the convergent numerator k_i which defines the number of complete circles. Thus, the return in the neighborhood of the initial state θ_0 takes place at the distance of $2\pi|\rho m_i - k_i|$ from the point θ_0 [14].

Let us consider the case when we start not from the point θ_0 but from the right boundary of its neighborhood, i.e., from the point $\theta'_0 = \theta_0 + \varepsilon_c/2$. The return in ε_c after the minimal number of iterations m_i happens near the left boundary of this neighborhood, i.e., at the point $\theta_0 - \varepsilon_c/2$. In such a case, as mentioned above, the point shifts by $2\pi|\rho m_i - k_i|$ from the initial position θ'_0 (see Fig. 2.4). This means that

$$\theta'_0 - 2\pi|\rho m_i - k_i| = \theta_0 - \varepsilon_c/2. \quad (2.17)$$

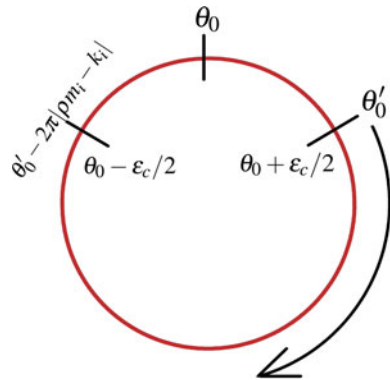
$$\theta_0 + \varepsilon_c/2 - 2\pi|\rho m_i - k_i| = \theta_0 - \varepsilon_c/2. \quad (2.18)$$

This enables one to derive the expression for calculating the value ε_i , which corresponds to the left boundary of the stairs step with the minimal return time $\tau_{\text{inf}} = m_i$ for any irrational rotation number ρ :

$$\varepsilon_i = \varepsilon_c = 2\pi|\rho m_i - k_i| \quad (2.19)$$

where ρ is the rotation number, m_i is convergent denominator, and k_i is the convergent numerator. As discussed above, the golden (silver) ratio represents a special case.

Fig. 2.4 Schematic representation of the neighborhood ε and initial and return points on the circle



The universal feature of the staircase dependence is due to the fact that numerators and denominators of convergents have the same definition rules and are elements of the Fibonacci (Pell) series. Thus, for the golden ratio, (2.19) can be rewritten as follows:

$$\varepsilon_i = 2\pi|\rho F_i - F_{i-1}|, \quad \text{or} \quad \varepsilon_i \approx \frac{2\pi}{L_i} \quad (2.20)$$

where F_i is the i th Fibonacci number, $\rho = (\sqrt{5} - 1)/2$ is the golden ratio, and L_i is the i th Lucas number.

Following the same motivation, for the silver ratio we can find

$$\varepsilon_i = 2\pi|\rho P_i - P_{i-1}| \quad \text{or} \quad \varepsilon_i \approx \frac{2\pi}{Q_i} \quad (2.21)$$

where P_i is the i th Pell number, $\rho = \sqrt{2} - 1$ is the silver ratio, and Q_i is the i th Pell–Lucas number.

We confirm our analytical results (2.19)–(2.21) by numerical simulation for the golden and silver ratios (Fig. 2.5) as well as for more complex Diophantine numbers $\sqrt[3]{2}$, e , and $\lg(5)$, which correspond to the absence of universal geometry of the step dependence (Fig. 2.6). Using (2.19), we can find the dependence of each step length D_i (Figs. 2.5 and 2.6) on its number in general.

For the golden and silver ratios, the length of stairs steps is constant and independent of the step number but is defined by the rotation number:

$$D_i = \text{const} = |\ln \rho|. \quad (2.22)$$

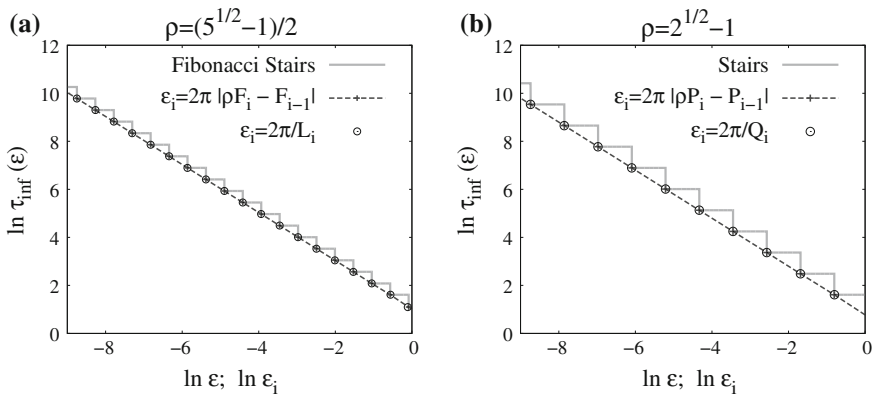


Fig. 2.5 Dependences $\ln \tau_{\text{inf}}(\ln \varepsilon)$ for **a** the golden ratio ($\rho = (\sqrt{5} - 1)/2$) and **b** the silver ratio ($\rho = \sqrt{2} - 1$) are indicated by *solid lines*; *dashed lines with plus points and circle points* represent the corresponding approximations using (2.20) for the golden ratio and (2.21) for the silver ratio

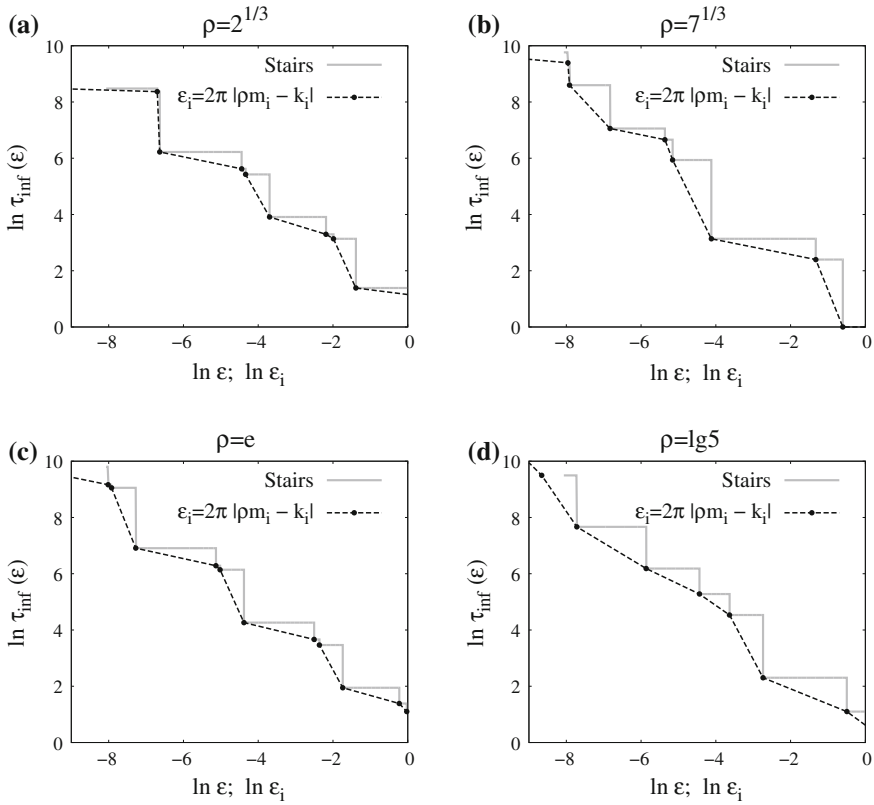


Fig. 2.6 Dependences $\ln \tau_{\text{inf}}(\ln \varepsilon)$ for four values of the rotation number: **a** $\rho = \sqrt[3]{2}$, **b** $\rho = \sqrt[3]{7}$, **c** $\rho = e$, and **d** $\rho = \lg 5$ (solid lines). Dashed lines with circle points show the corresponding approximations using (2.19)

Figure 2.7 illustrates dependences of the step length on the step number for the golden ratio (the universal geometry is valid) and for two different values of the rotation number, namely $\rho = \sqrt[3]{2}$ and $\lg 5$ (no universal geometry is observed). Figure 2.7a corresponds to the golden ratio and shows that all step lengths are equal. Figure 2.7b, c indicates that the universal geometry fails for the other rotation numbers. As shown in Fig. 2.7, analytical and numerical results are in full agreement. This means that the universal geometry can be obtained only in cases of the golden and silver ratios for which the step length does not depend on the step number (Fig. 2.7a).

Golden ratio.

In the case of the golden ratio ($\rho = (\sqrt{5} - 1)/2$), denominators and numerators of the convergents of ρ can be found as $m_i = F_i$ and $k_i = F_{i-1}$ where $\{F_i\}$ is the Fibonacci sequence. The golden ratio is a special case when numerators and denominators have the same determination rule and are elements of the same sequence. Thus, we can simplify the expression (2.19).

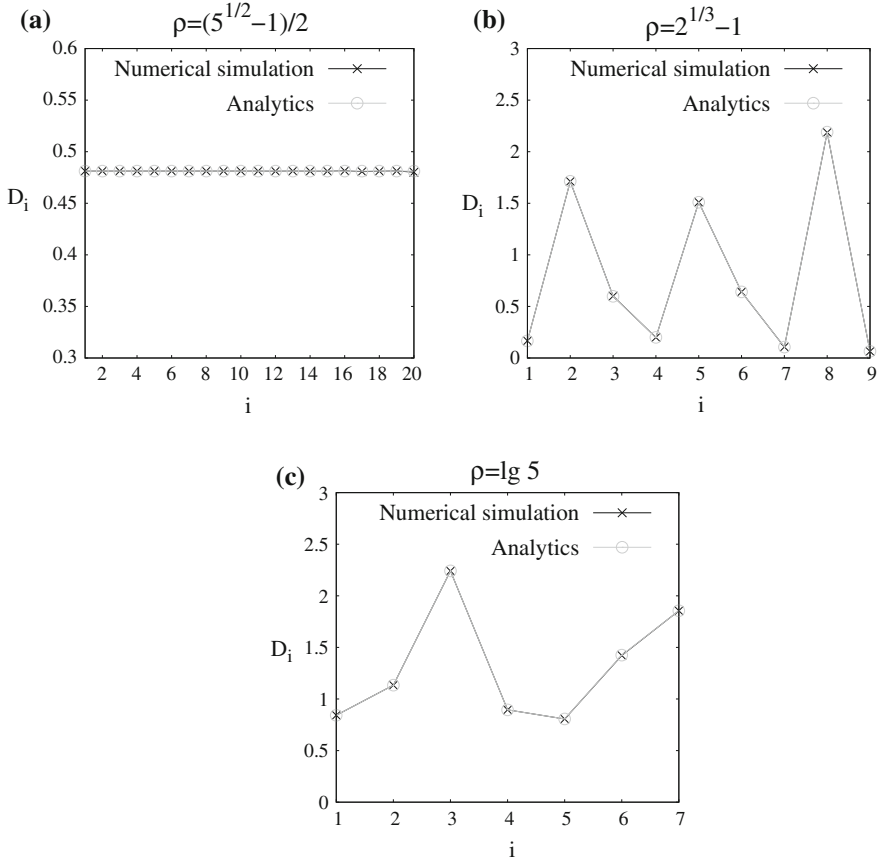


Fig. 2.7 Dependences of the step length on the step number for three values of the rotation number: **a** the golden ratio, **b** $\rho = \sqrt[3]{2}$, and **c** $\rho = \lg 5$

Each i th Fibonacci number is defined by the following recurrence relation:

$$F_i = F_{i-1} + F_{i-2} \quad (2.23)$$

with the set values $F_0 = 1$, $F_1 = 1$. The i th Fibonacci number can also be found using Binet's formula:

$$F_i = \frac{\varphi^i - (-\varphi)^{-i}}{2\varphi - 1} \quad (2.24)$$

where $\varphi = (\sqrt{5} + 1)/2$ is the root of the equation $\varphi^2 - \varphi - 1 = 0$ and depends on ρ as follows:

$$\rho = \varphi - 1 \quad \Leftrightarrow \quad \varphi = 1 + \rho. \quad (2.25)$$

The value of ε which corresponds to the emergence of a new stairs step and relates to the left boundary of the step with the minimal return time $\tau_{\inf} = F_i$ is

$$\varepsilon_i = 2\pi|\rho F_i - F_{i-1}|. \quad (2.26)$$

Using (2.24) and (2.25), this expression can be rewritten as follows:

$$\begin{aligned} \varepsilon_i &= 2\pi|(\varphi - 1)F_i - F_{i-1}| = 2\pi|\varphi F_i - (F_i + F_{i-1})| = \\ &= 2\pi|\varphi F_i - F_{i+1}| = 2\pi\left|\frac{\varphi^i - (-\varphi)^{-i}}{2\varphi - 1}\varphi - \frac{\varphi^{i+1} - (-\varphi)^{-i-1}}{2\varphi - 1}\right| = \\ &= 2\pi\left|\frac{\varphi^{i+1} + (-\varphi)^{-i+1} - \varphi^{i+1} + (-\varphi)^{-i-1}}{2\varphi - 1}\right| = \\ &= 2\pi\left|\frac{(-1)^{-i-1}(\varphi^{-i+1} + \varphi^{-i-1})}{2\varphi - 1}\right| = 2\pi|(-1)^{-i-1}| \times \\ &\quad \times \frac{\varphi^2 + 1}{2\varphi - 1}\varphi^{-i-1} = 2\pi\frac{\varphi^2 + 1}{2\varphi - 1}\varphi^{-i-1} = 2\pi\varphi^{-i}\frac{\varphi^2 + 1}{2\varphi^2 - \varphi} = \\ &= 2\pi\varphi^{-i}\frac{\varphi^2 - \varphi - 1 + \varphi + 2}{2\varphi^2 - \varphi - \varphi - 2 + 2 + \varphi} = 2\pi\varphi^{-i}\frac{\varphi + 2}{\varphi + 2} = 2\pi\varphi^{-i} = \\ &= \frac{2\pi\varphi^{-i}(\varphi^i + (-\varphi)^{-i})}{\varphi^i + (-\varphi)^{-i}} = \frac{2\pi}{\varphi^i + (-\varphi)^{-i}}(1 + (-1)^{-i}\varphi^{-2i}). \end{aligned} \quad (2.27)$$

Since $\varphi > 1$, the second term between the brackets tends to zero when $i \rightarrow \infty$. Thus,

$$\lim_{i \rightarrow \infty} \varepsilon_i(\tau_{\inf} = F_i) = \frac{2\pi}{\varphi^i + (-\varphi)^{-i}} = \frac{2\pi}{L_i} \quad (2.28)$$

where L_i is the i th Lucas number. It is defined by the same recurrence relation as the Fibonacci numbers (2.23) but with another set values $L_0 = 2$, $L_1 = 1$. The Lucas numbers can be approximately defined by the following formula:

$$L_i = \varphi^i + (-\varphi)^{-i}. \quad (2.29)$$

Calculation of the step length.

The size of the neighborhood ε_i , which corresponds to the left boundary of a step with the minimal return time $\tau_{\inf} = m_i$, for any irrational rotation number ρ can be found as follows:

$$\varepsilon_{Li} = \varepsilon_i = 2\pi|\rho m_i - k_i|. \quad (2.30)$$

Similarly, we can obtain the value ε_{i-1} . Since the dependence $\tau_{\inf}(\varepsilon)$ is a steplike function, ε_{i-1} is simultaneously the left boundary of the step with the minimal return time $\tau_{\inf} = m_{i-1}$ and the right boundary of the step with $\tau_{\inf} = m_i$:

$$\varepsilon_{Ri} = \varepsilon_{i-1} = 2\pi|\rho m_{i-1} - m_{i-1}|. \quad (2.31)$$

Hence, the length of the i th step of the dependence $\ln \tau_{\inf}(\ln \varepsilon)$ can be calculated as follows:

$$\begin{aligned}
D_i &= \ln \varepsilon_{Li} - \ln \varepsilon_{Ri} = \ln \frac{\varepsilon_{Li}}{\varepsilon_{Ri}} = \\
&= \ln \frac{2\pi |\rho m_i - k_i|}{2\pi |\rho m_{i-1} - k_{i-1}|} = \ln \frac{|\rho m_i - k_i|}{|\rho m_{i-1} - k_{i-1}|} = \\
&= \ln \frac{q_i |\rho - m_i/k_i|}{m_{i-1} |\rho - k_{i-1}/m_{i-1}|} \approx \ln \frac{m_i}{m_{i-1}}.
\end{aligned} \tag{2.32}$$

Thus, in general the length of stairs steps depends on denominators of convergents of rotation numbers. For the golden ratio, the denominators and numerators of the convergents are related to the Fibonacci series as $k_{i-1} = m_i = F_i$. It follows that for the golden ratio,

$$D_i \approx \ln \frac{m_i}{m_{i-1}} \approx \ln \frac{k_{i-1}}{k_{i-2}} \approx |\ln \rho|. \tag{2.33}$$

The same motivation can be used for the silver ratio. In this case, the numerators and denominators are connected with the Pell series: $k_{i-1} = m_i = P_i$. For this reason, the step lengths for the golden and silver ratios are constant and independent of the step number. They are defined only by the rotation number $|\ln \rho|$.

2.4 Afraimovich–Pesin Dimension for Different Rotation Numbers

The dependence $\tau_{\inf}(\varepsilon)$ obtained analytically enables one to define α_c more precisely. From (2.4) and (2.13), it follows that

$$\nu(\rho) = \alpha_c = 1. \tag{2.34}$$

Therefore, the AP dimension and the rate of approximation of the rotation number coincide and are equal to 1 in the case of the golden ratio.

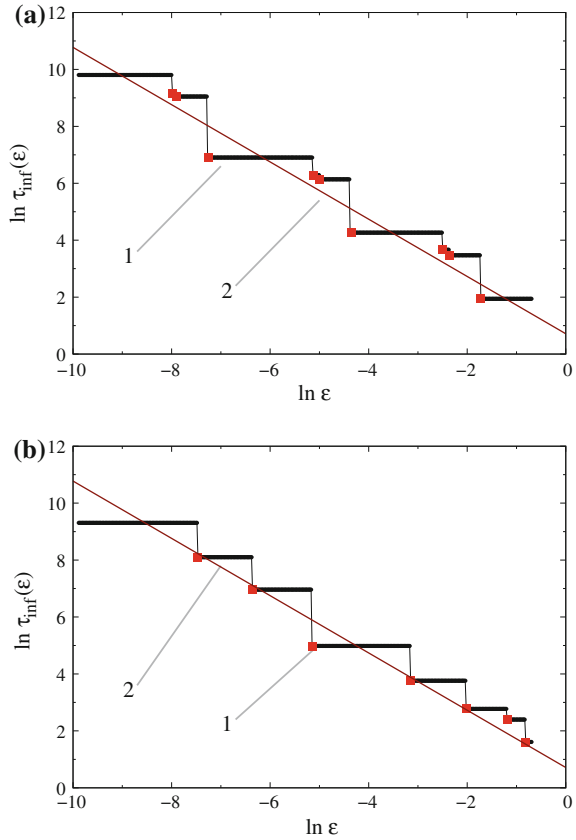
All the features described above are also valid in the case of the silver ratio. The dependence $\tau_{\inf}(\varepsilon)$ for the silver ratio is presented in Fig. 2.5b. The universal properties (2.15) and (2.16) of the Fibonacci stairs are also observed in this case. However, for the silver ratio, the sequence of minimal return times obeys the Pell law $m_{i+1} = 2m_i + m_{i-1}$ and forms the series: $\dots, 29, 70, 169, 408, 985, \dots$ [18]. Calculating the sequence of neighborhoods (2.21), we plot the dependence $\ln \tau_{\inf}(\varepsilon_i)$ which is also a straight line with slope -1 (Fig. 2.5b). Thus, in the case of the silver ratio, the AP dimension and the rate $\nu(\rho)$ are also equal to 1 as for the golden ratio.

The golden and silver ratios are algebraic Diophantine numbers with the measure of irrationality $\mu = 2$. It has been proven that any algebraic irrational number has $\mu = 2$ [19]. This means that (2.12), (2.13), and (2.34) hold for these numbers.

The universal geometry of the Fibonacci stairs is observed only for the golden and silver ratios and is attested to the peculiarities of their expansion in a continued fraction. This universal property is violated for other irrational rotation numbers.

Numerical results obtained for $\rho = \sqrt[3]{2}$ and $\rho = \sqrt[3]{7}$ are similar to the previous cases, but the Fibonacci stairs demonstrates a more complex structure.

Fig. 2.8 Calculation results for $\tau_{\text{inf}}(\varepsilon)$ in the map (2.6) for $K = 0$ and **a** $\rho = e$ and **b** $\rho = \pi/\sqrt{3}$. The Fibonacci stairs (curve 1), its linear approximation (curve 2). Plot 2 has slope 1

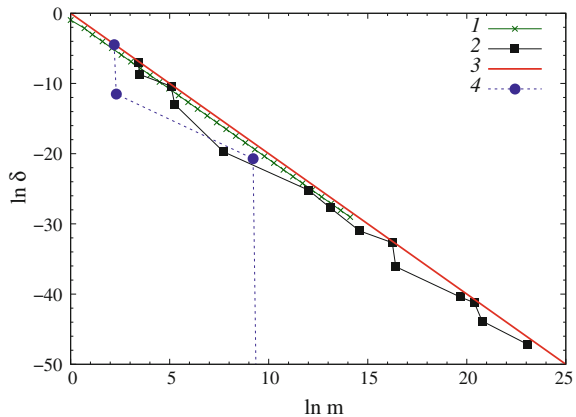


We now describe in detail transcendental numbers. It is known that any Liouvillian number is transcendental, but the opposite is not true, i.e., there are numbers that can be both Diophantine and transcendental simultaneously. These numbers have the measure of irrationality $\mu \geq 2$. Diophantine transcendental numbers can be exemplified by π , $\pi/\sqrt{3}$, $\pi/100$, e , $\ln 2$, $\ln 10$, and others. It has been proven that the number e has $\mu = 2$. There is only a theoretical estimation from above for the measure of the other numbers, e.g., $\mu(\pi) \leq 7.6063$, $\mu(\pi/\sqrt{3}) \leq 4.6016$, $\mu(\ln 2) \leq 3.57455391$. Figure 2.8 illustrates numerical results for $\pi/\sqrt{3}$ and e . Calculating the slope of the Fibonacci stairs by both averaging and theoretically gives $\nu(\rho) = \alpha_c = 1.0$. From a numerical viewpoint, this implies that both $\pi/\sqrt{3}$ and e are Diophantine numbers with the measure of irrationality $\mu = 2$.

It can be shown that the measure of irrationality for the irrational numbers considered takes exactly the values indicated above. Let us denote $\delta = |\rho - \frac{k}{m}|$ where k/m is a convergent of a continued fraction. In this case, (2.11) can be rewritten in the form

Fig. 2.9 Numerical data for the measure of irrationality μ for different numbers:

$\rho = (\sqrt{5} - 1)/2$ (curve 1),
 $\rho = \pi/\sqrt{3}$ (curve 2), the
theoretical approximation
 $\ln \delta = -2 \ln m$ (curve 3),
and $\rho = \lambda$ (curve 4)



$$\delta < \frac{C}{m^\mu}, \quad \text{or} \quad \ln \delta < \ln C - \mu \ln m. \quad (2.35)$$

The measure of irrationality can be determined as a slope of the dependence of $\ln \delta$ on $\ln m$ by calculating a sequence of nominators and denominators of convergents. Calculation results are shown in Fig. 2.9 for different irrational values of the rotation number. It is shown in the figure that $\mu = 2$ as in the previously considered cases of the golden and silver ratios, $\rho = e$, and $\rho = \pi/\sqrt{3}$. It follows that

$$\nu(\rho) = \mu(\rho) - 1. \quad (2.36)$$

This means that $\nu(\rho) = 1$ for $\mu = 2$. This fact confirms the numerical data for the unit AP dimension which are obtained for all the aforementioned values of the rotation number.

Transcendental Liouvillian numbers form a last subgroup of irrational numbers. They have a very high rate of convergence of rational approximations. In other words, their measure of irrationality is $\mu \rightarrow \infty$. We have considered several Liouvillian numbers, one of which is

$$\rho = \lambda = \sum_{i=0}^{\infty} 10^{-i!}. \quad (2.37)$$

The numerical results presented in Fig. 2.9 (curve 4) attest that $\mu \rightarrow \infty$ for $\rho = \lambda$. In this case, $\phi(t) \sim 1/t$ cannot be considered as a gauge function (Fig. 2.10). Unfortunately, we were not able to find an appropriate form for $\phi(t)$ in this case because of the finite computer accuracy. We have only found that (2.12) and (2.13) do not hold for Liouvillian irrational numbers and this fact corroborates the theoretical results [2, 4].

Fig. 2.10 Dependence of $\tau_{\text{inf}}(\varepsilon)$ for the Liouvillean rotation number $\rho = \lambda$

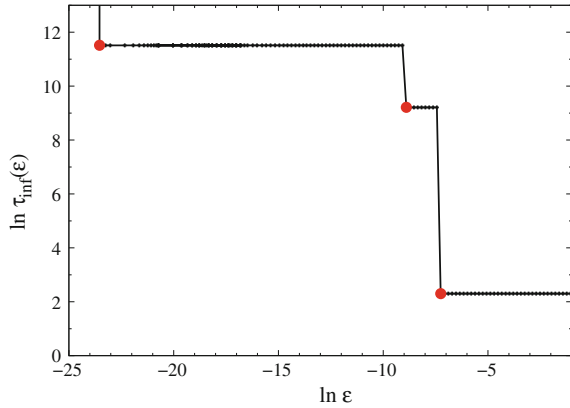
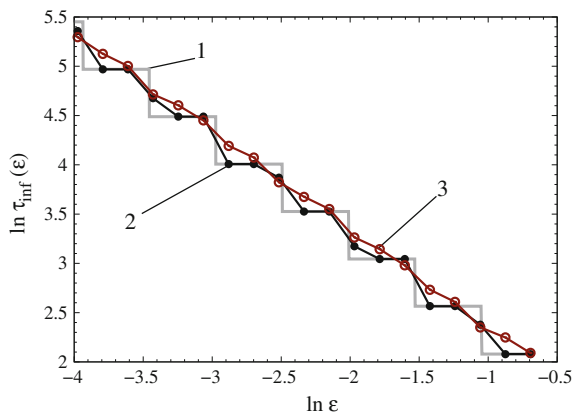


Fig. 2.11 Calculation results for $\ln \langle \tau_{\text{inf}}(\varepsilon) \rangle$ in the map (2.6) for $\rho = (\sqrt{5} - 1)/2$ and three different values of K : $K = 0$ (curve 1), $K = 0.1$ (curve 2), and $K = 0.6$ (curve 3)

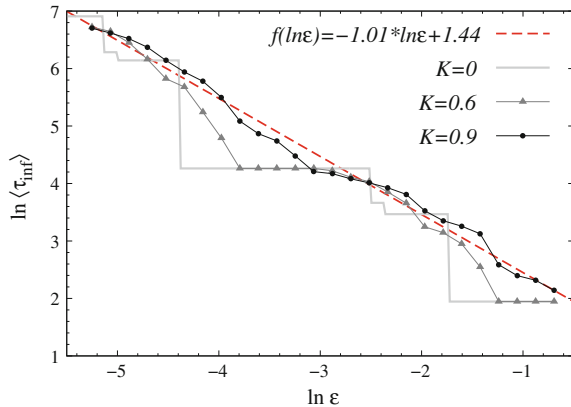


2.5 Impact of Nonlinearity

We now study the map (2.6) for $0 < K < 1$, i.e., when the system is nonlinear. For $K > 0$, the distribution density $p(\theta)$ is not uniform on the interval $0 \leq \theta \leq 2\pi$ (see Fig. 2.1). Therefore, to find $\langle \tau_{\text{inf}}(\varepsilon) \rangle$, one needs to divide the whole region on intervals of ε values and to calculate the mean value (2.1). We restrict ourselves to the case when the rotation number ρ is equal to the golden ratio. If K is varied in (2.6), ρ is also changed. Therefore, for fixed values of K , we select Δ in (2.6) so that $\rho = (\sqrt{5} - 1)/2$. Calculation data are shown in Fig. 2.11 for three different values of K .

Analysis of the data shown in Fig. 2.11 attests that when K grows, the Fibonacci stairs is gradually smoothing and practically tends to a straight line at $K = 0.6$. Calculations of the mean slope of the plots in Fig. 2.11 show that it is equal to -1 for $K = 0, 0.1$, and 0.6 . Thus, in the nonlinear case of the circle map (2.6), the AP dimension coincides with the rate $\nu(\rho)$ and is equal to $\nu(\rho) = \alpha_c = 1$. These

Fig. 2.12 Calculation results for $\ln\langle\tau_{\text{inf}}(\varepsilon)\rangle$ in the map (2.6) for $\rho = e$ and three different values of K : $K = 0$, $K = 0.6$, and $K = 0.9$



conclusions have been confirmed by numerical simulation with other values of the rotation number and for $0 < K < 1$. This is exemplified in Fig. 2.12 for $\rho = e$. It shows that the dependence $\ln\langle\tau_{\text{inf}}(\varepsilon)\rangle$ for $K = 0.9$ is a straight line with unit slope. It means that the AP dimension is equal to 1, $\alpha_c \approx 1.0$.

We note an important point. It is known that in the case of an irrational rotation number, the nonlinear circle map (2.6) can be transformed (or reduced) to the linear circle map $\psi_{n+1} = \psi_n + \Delta$ by using a suitable nonlinear change of variable $\psi = g(\theta)$ [6, 20]. This change must satisfy the property $g(\theta + 2\pi) = 2\pi + g(\theta)$. The result described above for the AP dimension $\alpha_c = 1$, which has been obtained both for the linear and the nonlinear circle map, testifies that the AP dimension is an invariant with respect to the nonlinear change of variables.

2.6 Fibonacci Stairs and the Afraimovich–Pesin Dimension for a Stroboscopic Section of a Nonautonomous van der Pol Oscillator

In addition to periodic oscillations, so-called quasiperiodic oscillations are widely and frequently encountered in nature and technology. Such oscillations are described by functions of the following form:

$$x(t) = \Phi[\gamma_1(\omega_1 t), \gamma_2(\omega_2 t) \dots \gamma_n(\omega_n t)] \quad (2.38)$$

where each function $f_n(\omega_n t)$ is periodic with period $T_n = 2\pi/\omega_n$. We are interested in quasiperiodic oscillations with two frequencies ω_1 and ω_2 . They are associated with a two-dimensional torus in the phase space. When the frequencies ω_1, ω_2 are rationally related, a resonance takes place on the torus and a limit cycle is realized. If the frequencies become irrationally related, the motion on the torus will be nonperiodic

or ergodic. The phase trajectory covers the torus surface everywhere densely and does not close as $t \rightarrow \infty$.

If we introduce a Poincaré secant plane which intersects a torus transversally, the points that appear when a trajectory intersects the plane generate a discrete sequence ψ_n lying on the closed curve. This sequence is described by the following equation [21, 22]:

$$\psi_{n+1} = \psi_n + \Delta + f(\psi_n) \quad (2.39)$$

where Δ is a shift of each subsequent point relative to the previous one and $f(\psi_n)$ is a certain periodic function. If only the first term of the expansion of $f(\psi_n)$ in a Fourier series is taken into account, the following discrete equation can be derived:

$$\psi_{n+1} = \psi_n + \Delta + K \sin \psi_n, \quad \text{mod } 2\pi. \quad (2.40)$$

The variable ψ_n can be treated as the coordinate of a point on the circle in the torus section, the parameter $\Delta = 2\pi\rho$ includes the rotation number ρ and characterizes the frequency detuning, and the parameter $0 < K < 1$ is related to the amplitude of oscillations at one of the independent frequencies. Equation (2.40) describes the circle map and serves as a classical model of nonlinear dynamics for modeling the dynamics of two-frequency quasiperiodic oscillations [21–25]. If the nonlinear term in (2.40) is neglected, one can come to the model of a linear circle shift

$$\psi_{n+1} = \psi_n + \Delta, \quad \text{mod } 2\pi, \quad \Delta = 2\pi\rho. \quad (2.41)$$

The circle map (2.40) is frequently used to study effects of synchronization and the transition to chaos via two-frequency oscillation destruction [26, 27].

The regime of two-frequency oscillations can be realized in several ways. For example, one can use two coupled self-sustained oscillatory systems with different basic frequencies. The simplest way consists in considering a self-sustained oscillatory system subjected to an external periodic force. Introducing the Poincaré secant plane of a two-dimensional torus results in a discrete set which must correspond to the circle map (2.40) for small values of the external amplitude. Alternatively, the circle map can be obtained by constructing a discrete set in the stroboscopic section of a phase trajectory through the period of the external force [21]. If the integration step $\Delta t = T/j$ where j is an integer, the set of points in this cross section is computed with maximum accuracy. This method is often known as the stroboscopic technique.

We consider a periodically driven van der Pol oscillator and apply the stroboscopic method to obtain a discrete set which is equivalent to the circle map. The next objective of our work is to show that the features of recurrence statistics established for the circle shift in the framework of the global theory can be reliably observed for the set in the stroboscopic section of the driven van der Pol oscillator. With this purpose, we construct the Fibonacci stairs and calculate the Afraimovich–Pesin dimension for different irrational values of the rotation number. In conclusion, we compare the theoretical results formulated for the circle shift (2.41) with our numerical data for the driven van der Pol oscillator.

2.6.1 System Under Study

The classical periodically driven van der Pol oscillator is described by the following equation:

$$\ddot{x} - (\alpha - x^2)\dot{x} + \omega_0^2 x = A \sin \Omega t. \quad (2.42)$$

We rewrite (2.42) in the form of a system of three first-order differential equations:

$$\begin{cases} \dot{x} = y, \\ \dot{y} = (\alpha - x^2)y - \omega_0^2 x + A \sin \Theta, \\ \dot{\Theta} = \Omega \end{cases} \quad (2.43)$$

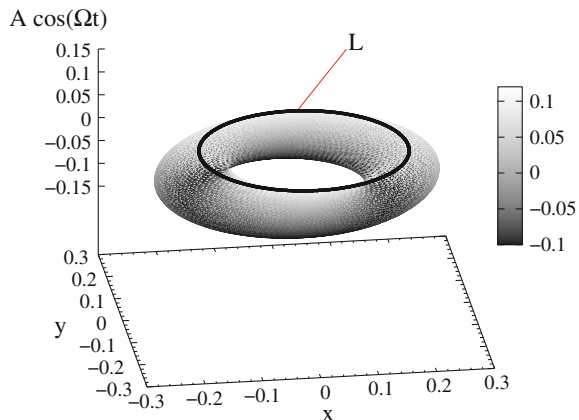
where α is the excitation parameter, ω_0 is the basic frequency of the self-sustained oscillations, A is the amplitude of the external force, $\Theta = \Omega t$ is the phase, and Ω is the frequency of the external force.

In contrast to the work [28], we do not pass to the equations for the amplitude and phase. Numerical simulation has shown that the calculation accuracy can be significantly increased by using the system (2.43) directly. This enables us to compare the theoretical and numerical results in more detail.

For $A \approx 0$ and $\alpha > 0$ in (2.42), a limit cycle is born with amplitude $2\sqrt{\alpha}$. In the three-dimensional system (2.43) for $A > 0$, we have quasiperiodic oscillations corresponding to a two-dimensional torus in the phase space. The torus can be ergodic or resonant depending on the ratio of frequencies ω_0 and Ω . We are interested in the case of an ergodic torus when the ratio of the frequencies (rotation number) is irrational.

We apply the stroboscopic technique to the system (2.43). This means that we observe the driven system at the times $t_j = j \cdot T$ where $T = \frac{2\pi}{\Omega}$ is the period of the external force and $j = 1, 2, \dots$. This observation results in the set of points shown in Fig. 2.13 together with a two-dimensional torus in the system (2.43). It is clearly shown in the figure that the map is quite equivalent to the circle shift.

Fig. 2.13 A two-dimensional torus and its stroboscopic section L in the system (2.43) for $\alpha = 0.01$, $\omega_0 = 1.0$, $\Omega = 1.1835944$, and $A = 0.1$



2.6.2 Numerical Results

In the general case of finite values of the external force amplitude $A > 0$, the set in the stroboscopic section corresponds to the nonlinear circle map (2.40):

$$\psi_{n+1} = \psi_n + \Delta + K(A) \sin \psi_n. \quad (2.44)$$

One can expect that for small $A \ll 1$, the coefficient $K(A)$ also satisfies the condition $K(A) \ll 1$, and in this case, the map (2.44) is similar to (2.41). Therefore, we are going to consider the cases of small and relatively large values of the amplitude of the external force A .

In order to compare the presented results with the theoretical data [2] and the calculations carried out in [15, 28], one needs to clarify the way of definition of the rotation number ρ .

The rotation number ρ can be defined as the mean increment of the angle ψ per one iteration of the circle map in relation to the total angle:

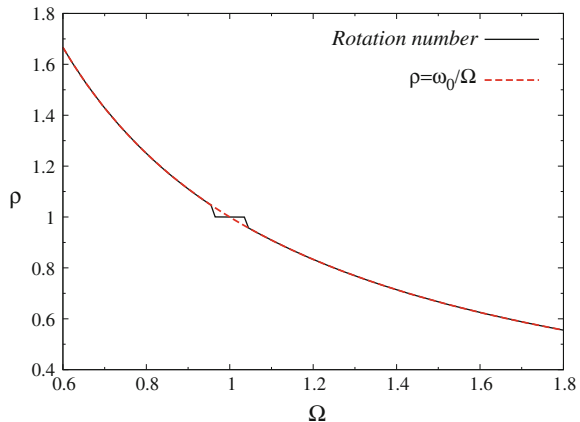
$$\rho = \lim_{n \rightarrow \infty} \frac{\psi_n - \psi_0}{2\pi n}. \quad (2.45)$$

It is easy to see that for $K(A) \rightarrow 0$, the parameter Δ in (2.44) represents a linear phase shift on a circle and is related to the rotation number as $\Delta = 2\pi\rho$. Moreover, in this case, the rotation number depends on the basic frequency ω_0 of the van der Pol oscillator and the frequency of the external force Ω . The dependence $\rho(\Omega)$ is shown in Fig. 2.14 for the fixed parameter values $\alpha = 0.01$, $\omega_0 = 1$, $A = 0.1$. As shown, the plot corresponds to the relation

$$\rho = \omega_0/\Omega \quad (2.46)$$

with the accuracy of $\pm 0.1\%$.

Fig. 2.14 Dependence of the rotation number ρ on the external frequency Ω in the system (2.43) for $\omega_0 = 1$, $\alpha = 0.01$, and $A = 0.01$



When $\omega_0 = \Omega = 1$, the resonance 1 : 1 can be observed in Fig. 2.14. The theoretical curve must have an infinite number of “plateaus” which correspond to resonances $\omega_0/\Omega = l/q$ where $l, q = 1, 2, \dots$. This curve is called the “devil’s staircase” [29]. However, high-order resonances ($q > 1$) are not visible in the scale of Fig. 2.14 because they can be observed only within the narrow intervals with respect to Ω , and the external amplitude is much less than the amplitude of oscillations in the van der Pol oscillator.

2.6.2.1 The Case of Small Values of the External Amplitude

We now consider the case of small values of the external amplitude ($A = 10^{-5}$). The set in the stroboscopic section of the system (2.43) is shown in Fig. 2.15a on the plane of variables (x_s, y_s) . It looks like a circle with radius $r = \sqrt{x_s^2 + y_s^2}$. Since for $\alpha = 0.01$ the amplitude $r = 0.2$ is constant, the sequence of phase shifts ψ_n can be analyzed in the polar system of coordinates: $x_{sn} = r \cos \psi_n$, $y_{sn} = r \sin \psi_n$.

The set of values ψ_n must satisfy the circle map (2.44). Let us consider the case of small values of the external amplitude $A \ll 1$. Figure 2.15b shows the probability distribution density $p(x_s, y_s)$ of points on the circle (Fig. 2.15a) for the golden ratio $\rho = (\sqrt{5} - 1)/2$. As shown in the figure, $p(x_s, y_s)$ is rather uniform and corresponds to the linear circle shift (2.41). If this is true, then only local approach can be used to calculate $\langle \tau_{\text{inf}}(\varepsilon) \rangle$ by varying ε in a certain interval (for any point on the circle). This is related to the fact that for a uniform distribution, $\tau_{\text{inf}}(\varepsilon)$ is independent of the choice of ε on the circle length. The calculation results for $\tau_{\text{inf}}(\varepsilon)$ are presented in Fig. 2.16 for the golden ratio. In contrast to the results of [28], in a wide range of ε values, the numerical plot in Fig. 2.16 is qualitatively and quantitatively consistent with the calculation data for the linear circle map (2.41), which are presented in Fig. 2.2a. This is due to an increase of the calculation accuracy of the stroboscopic section.

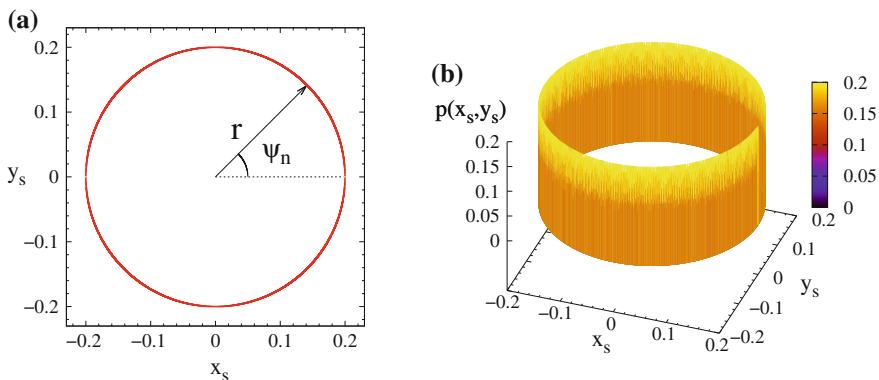


Fig. 2.15 The stroboscopic section (a) and the probability distribution density $p(x_s, y_s)$ on the circle (b) for $\alpha = 0.01$, $\omega_0 = 1$, $A = 10^{-5}$. The value $\Omega = 1.6180141526367187$ corresponds to the golden ratio $\rho = (\sqrt{5} - 1)/2$

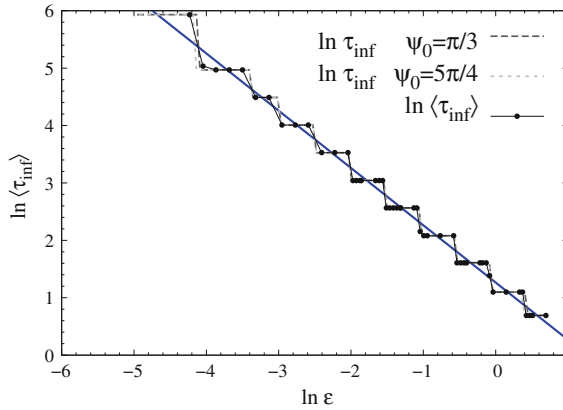


Fig. 2.16 The Fibonacci stairs for the stroboscopic section of phase trajectories in the system (2.43) for $\alpha = 0.01$, $\omega_0 = 1.0$, $A = 10^{-5}$, $\rho = \omega_0/\Omega$, and $\Omega = 1.6180141526367187$. The curve with points corresponds to the global approach; *dashed lines* are constructed by using the local approach when recurrences are calculated in neighborhoods of the points $\psi_0 = \pi/3$ and $\psi_0 = 5\pi/4$. All curves are approximated by a *straight line* with slope $\alpha_c = 1$

Comparing Figs. 2.2a and 2.16 reveals that all the dependences coincide in the range $-4 < \ln \varepsilon < 1$. The sequence of τ_{inf} on the steps of the Fibonacci stairs in Fig. 2.16 strictly complies with the basic Fibonacci series. The height and width of the stairs steps are $D_i \simeq |\ln \rho|$. The average slope of the linear approximation is equal to -1 and gives the AP dimension $\alpha_c = 1$. When $\ln \varepsilon < -4$, the Fibonacci stairs is gradually destroyed. This is due to the accuracy of calculations and to the fact that the distribution density $p(x_s, y_s)$ becomes inhomogeneous for sufficiently small ε . Nearly identical results have been obtained for the external amplitude taken in the range $10^{-8} \leq A \leq 10^{-3}$. One may say that for small values of $A \leq 10^{-3}$, the map in the stroboscopic section has the properties of the circle shift (2.41) with a rather high degree of accuracy.

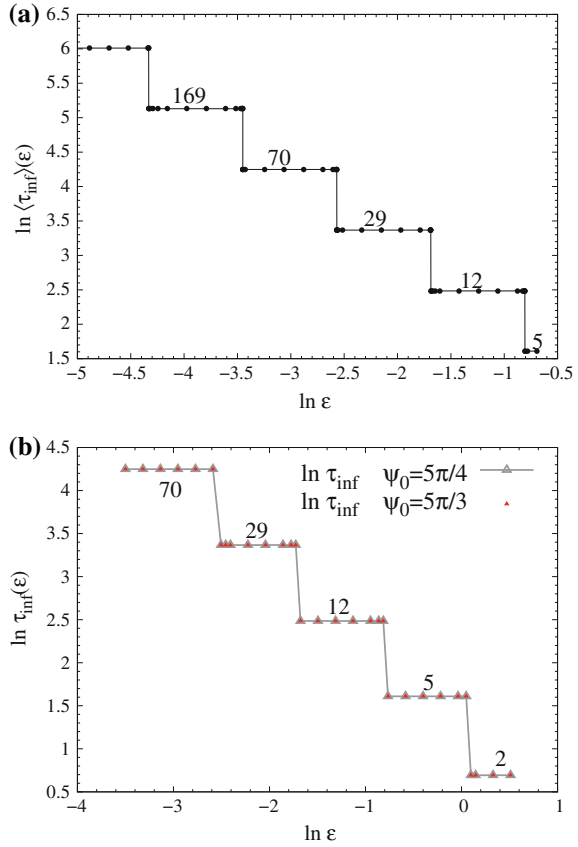
To confirm the results described above, we consider the case of the silver ratio $\rho = \sqrt{2} - 1$. The corresponding numerical results are shown in Fig. 2.17. In this case, the frequency of the external force is set to be $\Omega = 0.414209134578705$.

Since the external amplitude $A = 10^{-8}$ is very small, the numerical data in Fig. 2.17a, b demonstrate their good qualitative and quantitative agreement. The sequence of $\tau_{\text{inf}}(\varepsilon)$ on the stairs steps corresponds to the basic Pell series. The height and width of the steps are $D_i \simeq |\ln \rho|$.

2.6.2.2 The Case of Relatively Large Values of the External Amplitude

We now turn to relatively large values of the external amplitude $A > 10^{-3}$. In this case, the nonlinear item $K(A)$ in the circle map (2.44) may effect the results. The numerical data are shown in Fig. 2.18 for $A = 10^{-2}$. The distribution density

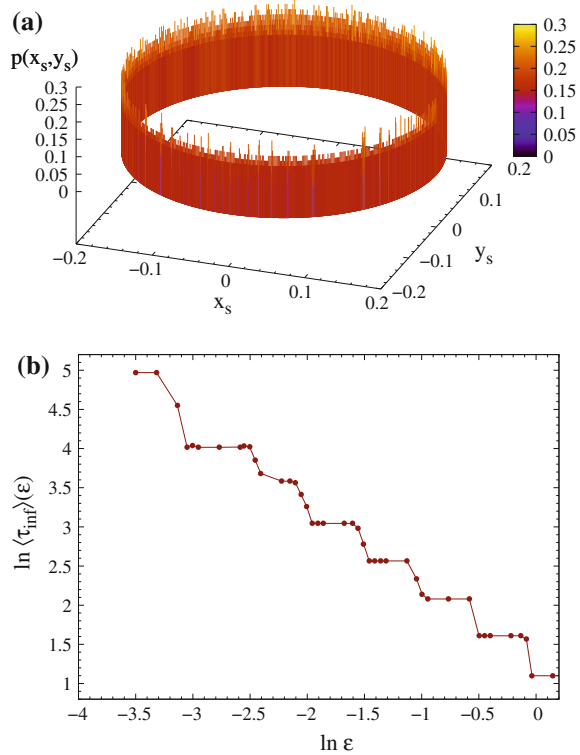
Fig. 2.17 The Fibonacci stairs **a** for the linear circle map (2.41) with $\Delta = 2\pi\rho$, $\rho = \sqrt{2} - 1$ and **b** for the map in the stroboscopic section of the system (2.43) for $\alpha = 0.01$, $\omega_0 = 1$, $A = 10^{-8}$, $\rho = \omega_0/\Omega$, and $\Omega = 0.414209134578705$



$p(x_s, y_s)$ becomes nonuniform (Fig. 2.18a), and $\langle \tau_{\text{inf}}(\epsilon) \rangle$ must be found by covering the whole set with intervals of size ϵ and then averaging the calculation data. As shown in Fig. 2.18b, if the external amplitude A increases, the Fibonacci stairs begins to break down. The average slope of the graph is approximately equal -1 , i.e., the AP dimension retains the value of $\alpha_c = 1$. When A is further increased, the plot in Fig. 2.18b tends to a straight line with slope $\simeq -1$, as in the case of the nonlinear circle map (2.44) studied in [28].

We have also carried out numerical calculations for another values of the rotation number ρ by varying the external frequency Ω . The obtained results fully comply with the data described in [28], namely the Fibonacci stairs for another Diophantine rotation numbers loses its universal properties established for the golden and silver ratios. However, the AP dimension remains close to 1 ($\alpha_c \simeq 1.0$) both for small and relatively large values of the external amplitude $10^{-8} \leq A \leq 10^{-2}$. Figure 2.19 exemplifies the Fibonacci stairs calculated for the Diophantine rotation number $\rho = \sqrt[3]{2}$.

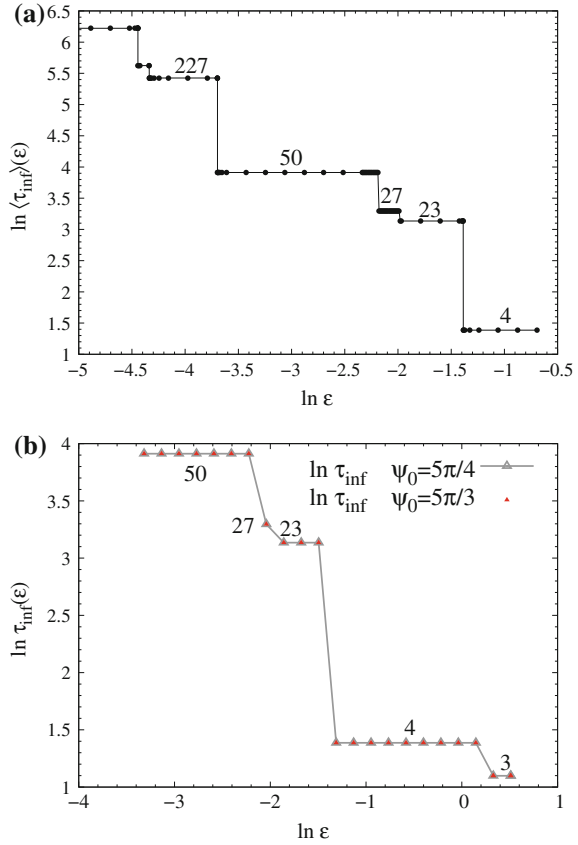
Fig. 2.18 The probability distribution density (a) and the Fibonacci stairs (b) for the map in the stroboscopic section of the system (2.43) for $\alpha = 0.01$, $\omega_0 = 1$, $A = 10^{-2}$, and $\rho = (\sqrt{5} - 1)/2$



Comparison of the plots in Fig. 2.19a, b testifies a good correspondence of the results. The average value of the slope of these graphs is close to -1 (-0.98 ± 0.01).

In this section, the results of the global analysis of Poincaré recurrence statistics have been presented for the set in the stroboscopic section of the driven van der Pol oscillator through the period of the external force. It has been established that this set can be described by the circle map (2.44) with the irrational rotation number $\rho = \omega_0/\Omega$. It has been shown that the stroboscopic map is close to the linear circle shift (2.41) in the case of small values of the external amplitude $A \ll 1$, while for relatively large values of A , it corresponds to the nonlinear circle map (2.44) due to the nonlinearity. The AP dimension is $\alpha_c \simeq 1$ in both cases. Our numerical simulation has confirmed the universal nature of the Fibonacci stairs (Figs. 2.16 and 2.17) for the golden and silver ratios. The height and width of the stairs steps have been numerically obtained to be equal to $D_i = |\ln \rho|$. The universality of the Fibonacci stairs is violated for other values of the rotation number (see Fig. 2.19). These results completely confirm the data obtained numerically for the map (2.44). The fact that the AP dimension remains equal to 1 both in the linear and nonlinear cases is caused by the invariance of the AP dimension with respect to a nonlinear change of coordinates. As discussed in [28], the map (2.44) can be reduced to the circle shift (2.41) by a suitable change of variables [21].

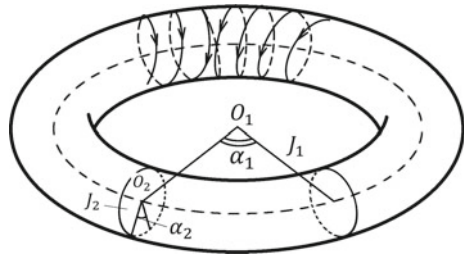
Fig. 2.19 The Fibonacci stairs **a** for the linear circle map (2.41) with $\Delta = 2\pi\rho$, $\rho = \sqrt[3]{2}$ and **b** for the map in the stroboscopic section of (2.43) for $\alpha = 0.01$, $\omega_0 = 1$, $A = 10^{-8}$, and $\rho = \sqrt[3]{2}$



2.7 Poincaré Recurrences in Hamiltonian Systems

Different fractal objects can be observed in the phase space of Hamiltonian systems. They have a complex structure which indicates the complexity in the system behavior [4]. For this reason, this type of systems can be rather interesting to analyze in terms of description of Poincaré recurrence statistics. From the standpoint of Poincaré recurrence theory, Hamiltonian systems were explored long ago [30], while they have only been recently studied in the framework of multifractal analysis [3, 4, 31–33]. The cited works are mainly based on the study of the probability distribution of recurrences which are obtained by using the method of multifractal analysis [4]. Hamiltonian systems can be exemplified by the Hénon–Heiles model [34], scattering billiards (Sinai billiards), a periodically kicked rotator, a double pendulum [35], and several discrete-time systems [3, 4, 36].

Fig. 2.20 Schematic representation of the phase space of a system with two degrees of freedom



Let us consider one of such systems, namely a periodically driven nonlinear conservative oscillator which is described by the following equations:

$$\begin{aligned}\dot{x} &= y, \\ \dot{y} &= -\sin x + b \sin \Theta, \\ \dot{\Theta} &= \Omega\end{aligned}\tag{2.47}$$

where the oscillation amplitude of the autonomous oscillator is equal to 1 and its frequency is $\omega_0 = 1$. The external force is defined by the amplitude b and frequency Ω . When the variables “action—angle” are used (if the canonic transformation $(\vec{q}, \vec{p}) \rightarrow (\vec{\alpha}, \vec{J})$ is possible), the dynamics of such systems can be visibly represented as follows: the circular motion with the center at O_1 , which is formed by the α_1, J_1 variables, and simultaneously the rotation along the circle centered at O_2 (lying in the plane which is transversal to the plane of the O_1 circle), which is formed by the α_2, J_2 variables (Fig. 2.20). The superposition of these rotations defines the motion on a two-dimensional torus.

The behavior of phase trajectories depends crucially on the frequency ratio Ω/ω_0 . If the ratio is rational, i.e., $\Omega/\omega_0 = k/m$ where k and m are integers, then in a certain time $T = 2\pi(k\Omega + m/\omega_0)$, the trajectory returns to the point which it leaves at the time $t_0 = t - T$. When the frequencies are irrationally related, the phase trajectory does not close on itself and covers the torus surface everywhere densely.

Phase portraits for the system (2.47) are shown in Fig. 2.21 (left column) for several values of the parameter b . Starting with a certain value of b , quasiperiodic and chaotic motions in the phase portrait become indistinguishable, so that we continue analyzing the Hamiltonian dynamics by applying the stroboscopic technique, i.e., we fix a sequence of points through the interval 2π on the phase variable Θ . In this case, periodic motions will be associated with a finite sequence of points, quasiperiodic motions—with closed trajectories, and chaotic behavior—with a random sequence of points. Related sets of points in the stroboscopic section of the system (2.47) are depicted in Fig. 2.21 (right column).

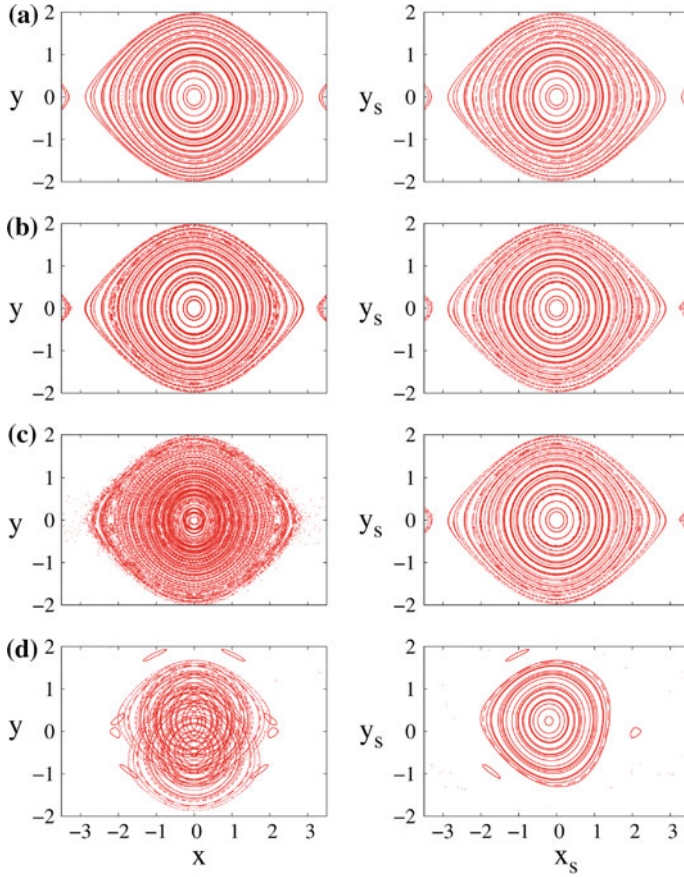


Fig. 2.21 Phase portraits (*left column*) and the corresponding sets of points in the stroboscopic section (*right column*) of the system (2.47) for $\Omega = 2\pi/3$ and different values of the parameter b : (a) $b = 0.001$, (b) $b = 0.01$, (c) $b = 0.1$, and (d) $b = 0.8$

2.7.1 Poincaré Recurrences in a Periodically Driven Nonlinear Conservative Oscillator

Let us consider what happens with the dependence $\ln\langle\tau_{\text{inf}}(\varepsilon)\rangle$ (2.13) in the case of Hamiltonian systems. We first fix $b = 0.001$ that corresponds to Fig. 2.21a. In this case, the phase portrait and the stroboscopic section look like a set of circles and ellipses with different radii. Falling on a particular set of points depends on initial conditions, so we fix the initial conditions as $x_0 = 0.44$ and $y_0 = 0$ which correspond to a circle with a constant radius ≈ 0.2 . Thus, we can further turn to the polar system of coordinates and consider only one variable—the angle ψ instead of a pair of coordinates (x, y) . Figure 2.22 illustrates the dependence of the rotation

Fig. 2.22 The rotation number ρ as a function of the external frequency Ω in the system (2.47) for $b = 0.001$ and initial conditions $x_0 = 0.44$ and $y_0 = 0$

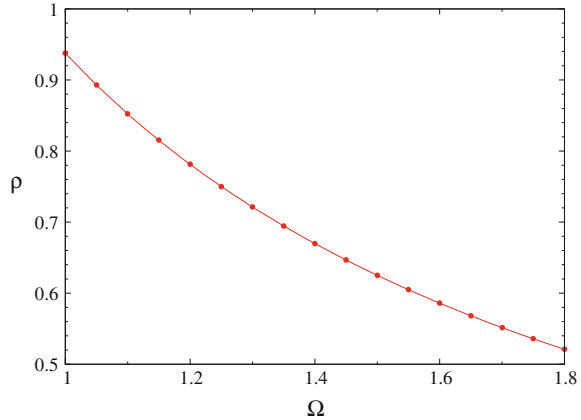
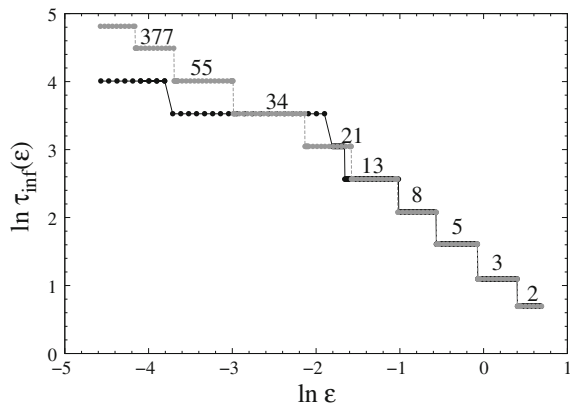


Fig. 2.23 Dependence of the minimal Poincaré return time on the size of the return region (local approach) in the system (2.47) for $b = 0.001$; $\Omega = 1.598233989$; and initial conditions $x_0 = 0.44$ and $y_0 = 0$. The *black curve* corresponds to the return vicinity of the point $\psi_0 = \pi/3$ and the *gray curve*—to the return region of the point $\psi_0 = 2\pi/3$



number on the external frequency Ω for the system (2.47). This plot is quite similar to that for $\rho = 1/\Omega$. On this basis, one can choose a value of Ω so that the rotation number is close to the golden ratio. However, one must take into account the fact that in Hamiltonian systems, frequencies and, consequently, rotation numbers depend strongly on the radius of a circle. This enables one to set the rotation number only with a certain error.

Figure 2.23 shows the dependence of minimal Poincaré return times (local approach) on the size ε of a return vicinity for two initial states $\psi_0 = 2\pi/3$ and $\psi_0 = \pi/3$. As shown in the figure, the dependences begin to diverge starting from the step with number 13.

Such a difference in the dependences results from the fact that even at $b = 0.001$ the probability distribution density is nonuniform (see Fig. 2.24). This implies that the local approach cannot be applied in the case of $b = 0.001$. Figure 2.25 shows the dependence $\tau_{\text{inf}}(\varepsilon)$ calculated using the global approach. It shows that the stairs

Fig. 2.24 Probability distribution density $p(\psi)$ in the system (2.47) for $b = 0.001$ and initial conditions $x_0 = 0.44$ and $y_0 = 0$

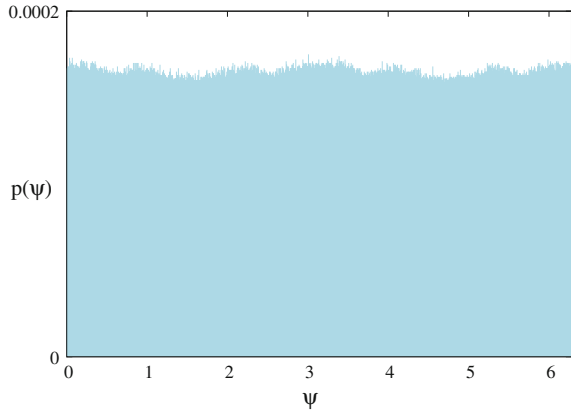
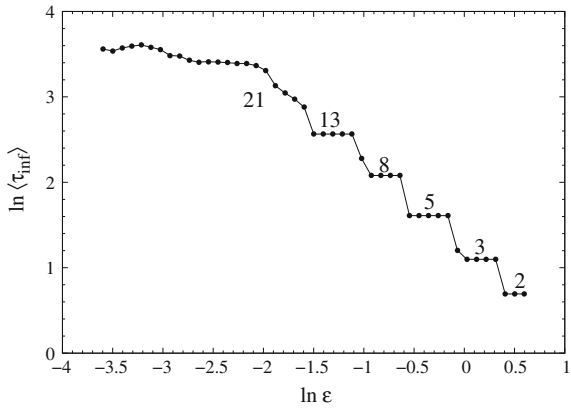


Fig. 2.25 Dependence of the mean minimal Poincaré return time on the vicinity size in the global approach for the system (2.47) at $b = 0.001$ and $\Omega = 1.598233989$



is destroyed also starting from the step $\langle \tau_{\text{inf}}(\varepsilon) \rangle = 13$. This is caused by a too large amplitude of the external force.

Calculation results for the local and global approaches are shown in Fig. 2.26 for $b = 0.00001$. As follows from the figure, when the global approach is applied, the staircase is broken later (from the step with number 34).

We may conclude that the dynamics of points on circles in Hamiltonian systems demonstrate the same regimes as the circle map. For a small external amplitude, the dependence $\tau_{\text{inf}}(\varepsilon)$ represents the Fibonacci stairs which is destroyed when the external amplitude b increases. It should be noted that for different rotation numbers and regardless of the nonlinearity degree of an invariant closed curve in (2.47), the AP dimension α_c turns out to be equal to unity in full compliance with the theory [2, 4]. The AP dimension is defined by the slope of the linear approximation of the step functions (Figs. 2.23, 2.25, and 2.26) in the range of ε values when the Fibonacci stairs is not yet destroyed.

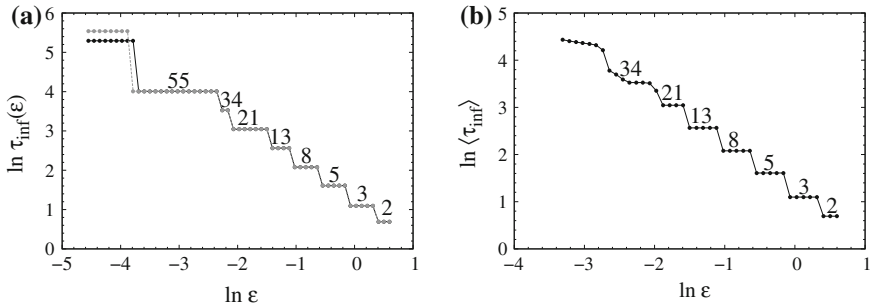


Fig. 2.26 **a** Dependence of the minimal Poincaré recurrence time on the vicinity size (local approach) in the system (2.47) for $b = 0.00001$; $\Omega = 1.598033989$; and initial conditions $x_0 = 0.44$, $y_0 = 0$. The black curve corresponds to the return vicinity of the point $\psi_0 = \pi/3$ and the gray curve—to the return region of the point $\psi_0 = 2\pi/3$. **b** Dependence of the mean minimal Poincaré recurrence time on the vicinity size (global approach) in the system (2.47) for $b = 0.00001$ and $\Omega = 1.598033989$

2.8 Conclusion

In the present work, we have described the numerical results for the statistics of Poincaré recurrence sequences in ergodic sets without mixing. We have considered sets in the dissipative circle map and in stroboscopic sections of the nonautonomous van der Pol oscillator and nonautonomous conservative oscillator. It has been found that in all the above examples, regardless of the nonlinearity degree, the Afraimovich–Pesin dimension is $\alpha_c = 1$, that is fully consistent with the theory developed for the linear circle shift [2, 4]. We have established that the dependence of $\ln \tau_{\text{inf}}(\varepsilon)$ on $\ln \varepsilon$ represents a step function and have substantiated theoretically its geometric properties. The universal geometry of the above dependence has been proven for the golden and silver ratios. The length and the height of the Fibonacci stairs steps are defined by $|\ln \rho|$ [15, 16]. The universality of the Fibonacci stairs is violated if rotation numbers are different from the golden and silver ratios as well as in cases caused by the growth of nonlinearity degree of the systems under consideration.

Acknowledgements This work was supported by RFBR (Grants No. 14-52-12002 and No. 15-02-02288) and the Russian Ministry of Education and Science (project code 1008).

References

1. Nemytskii, V.V., Stepanov, V.V.: Dover Books on Mathematics. Dover Publications, New York (1989)
2. Afraimovich, V.: Chaos **7**(1), 12 (1997)
3. Afraimovich, V., Zaslavsky, G.: Phys. Rev. E **55**, 5418 (1997)

4. Afraimovich, V., Ugalde, E., Urias, J.: *Fractal Dimension for Poincaré Recurrences*. Elsevier, Amsterdam (2006)
5. Kac, M.: *Bull. Am. Math. Soc.* **53**(10), 1002 (1947)
6. Hirata, M., Saussol, B., Vaienti, S.: *Commun. Math. Phys.* **206**(1), 33 (1999)
7. Penné, V., Saussol, B., Vaienti, S.: *J. de Physique (Paris) Proceedings of the Conference "Disorders and Chaos"*, Rome **08**(6), 163 (1998)
8. Anishchenko, V., Astakhov, S., Boev, Y., Biryukova, N., Strelkova, G.: *Commun. Nonlinear Sci. Numer. Simul.* **18**(12), 3423 (2013)
9. Anishchenko, V.S., Astakhov, S.V.: *Uspekhi Fizicheskikh Nauk* **56**(10), 955 (2013)
10. Afraimovich, V., Lin, W., Rulkov, N.: *Int. J. Bifurc Chaos* **10**(10), 2323 (2000)
11. Anishchenko, V., Khairulin, M., Strelkova, G., Kurths, J.: *Eur. Phys. J. B* **82**, 219 (2011)
12. Pettofrezzo, A.J., Byrkit, D.R.: *Prentice-Hall* (1970)
13. Slater, N.: *Proc. Camb. Philos. Soc.* **63**(4), 1115 (1967)
14. Buric, N., Rampioni, A., Turchetti, G.: *Chaos, Solitons Fractals* **23**(5), 1829 (2005)
15. Anishchenko, V., Semenova, N., Vadivasova, T.: *Discontinuity, Nonlinearity Complexity* **4**(2), 111 (2015)
16. Semenova, N., Rybalova, E., Anishchenko, V.: *Discontinuity, Nonlinearity and Complexity* (2016)
17. Anishchenko, V.S., Boev, Y.I., Semenova, N., Strelkova, G.: *Phys. Rep.* **587**, 1 (2015)
18. Bicknell, M.: *Fibonacci Q.* **13**(4), 345 (1975)
19. Roth, K.: *Mathematika* **2**(1), 1 (1955)
20. Denjoy, A.: *Math. Pures Appl.* **11**(9), 333 (1932)
21. Pikovsky, A., Rosenblum, M., Kurths, J.: *Synchronization: A Universal Concept in Nonlinear Sciences*. Cambridge University Press, Cambridge (2002)
22. Kuznetsov, S.: *Dynamical Chaos*. Fizmatlit, Moscow (2001)
23. Arnold, V.: *Am. Math. Soc. Transl.* **2**(46), 213 (1965)
24. Ott, E.: *Chaos in Dynamical Systems*. Cambridge University Press, Cambridge (1992)
25. Schuster, H.G.: *Deterministic Chaos*. Physik-Verlag (1984)
26. Boyland, P.: *Commun. Math. Phys.* **106**(3), 353 (1986)
27. Rand, D., Ostlund, S., Sethna, J., Siggia, E.: *Phys. Rev. Lett.* **49**, 132 (1982)
28. Semenova, N., Vadivasova, T., Strelkova, G., Anishchenko, V.: *Commun. Nonlinear Sci. Numer. Simul.* **22**, 1050 (2015)
29. Rasband, S.N.: *Chaotic Dynamics of Nonlinear Systems*. Wiley (1990)
30. Chirikov, B.V., Shepelyansky, D.L.: *Physica D* **13**, 395 (1984)
31. Chirikov, B.V., Shepelyansky, D.L.: *Phys. Rev. Lett.* **82**, 528 (1999). doi:[10.1103/PhysRevLett.82.528](https://doi.org/10.1103/PhysRevLett.82.528)
32. Chirikov, B.V., Shepelyansky, D.L.: *Phys. Rev. Lett.* **89**, 239402 (2002). doi:[10.1103/PhysRevLett.89.239402](https://doi.org/10.1103/PhysRevLett.89.239402)
33. Shepelyansky, D.L.: *Phys. Rev. E* **82**, 055202 (2010). doi:[10.1103/PhysRevE.82.055202](https://doi.org/10.1103/PhysRevE.82.055202)
34. Lichtenberg, A., Leiberman, M.: *Regular and Stochastic Motion*. Applied Mathematical Sciences. Springer, Berlin (1982)
35. Srivastava, N., Kaufman, C., Müller, G.: *Comput. Phys.* **4**, 549 (1990)
36. Feudel, U., Grebogi, C., Hunt, B.R., Yorke, J.A.: *Phys. Rev. E* **54**, 71 (1996). doi:[10.1103/PhysRevE.54.71](https://doi.org/10.1103/PhysRevE.54.71)

Regularity and Stochasticity of Nonlinear Dynamical
Systems

Volchenkov, D.; Leoncini, X. (Eds.)

2018, X, 311 p. 99 illus., 79 illus. in color., Hardcover

ISBN: 978-3-319-58061-6